Synthesis, Structure, and Spectroscopy of Rare Earth Hypophosphites. Part 2. Uranyl Hypophosphite Monohydrate and Uranyl Hypophosphite—Hypophosphorous Acid (1/1)

ARTICLE *in* INORGANIC CHEMISTRY · JANUARY 2000

Impact Factor: 4.76 · DOI: 10.1021/ic990188r · Source: PubMed

2 AUTHORS, INCLUDING:

Peter Anthony Tanner
The Hong Kong Institute of Education
355 PUBLICATIONS **4,367** CITATIONS

SEE PROFILE

Synthesis, Structure, and Spectroscopy of Rare Earth Hypophosphites. 2. Uranyl Hypophosphite Monohydrate and Uranyl Hypophosphite−Hypophosphorous Acid (1/1)

Peter A. Tanner*,[1a] and Thomas C. W. Mak[1b]

Department of Biology and Chemistry, City University of Hong Kong, Tat Chee Avenue, Kowloon, Hong Kong SAR, and Department of Chemistry, The Chinese University of Hong Kong, Shatin, New Territories, Hong Kong SAR

Received February 17, 1999

The new compounds $UO_2(H_2PO_2)_2 \cdot H_2O$ (**1**) and $UO_2(H_2PO_2)_2 \cdot H_3PO_2$ (**2**) crystallize in the space groups $P2_1/n$ and $P2_12_12_1$, respectively, each with $Z = 4$. For **1**, $a = 7.686(2)$ Å, $b = 9.275(2)$ Å, $c = 11.027(2)$ Å, $\alpha = 90°$, $\beta = 92.32(3)°$, $\gamma = 90°$; for **2**, $a = 7.1572(4)$ Å, $b = 7.2363(6)$ Å, $c = 17.554(2)$ Å, $\alpha = \beta = \gamma = 90°$. Each uranium atom, situated at a general position, has a distorted pentagonal bipyramidal coordination geometry, and U−O−P−O−U bridges form differently oriented chains in **1** and a three-dimensional network structure in **2**. H_3PO_2 serves as a terminal monodentate ligand in **2**. The infrared and Raman spectra of **1** and **2** show (i) characteristic uranyl modes of vibration; (ii) partially resolved unit cell group modes of hypophosphite anions; and (iii) bands due to water and H_3PO_2, respectively. The C_1 site symmetry in these compounds makes their spectral properties useful in evaluating the presence of additional electronic transitions not identified in the analyses of higher symmetry uranyl compounds. In the region between 20 000 and 29 000 cm^{-1}, 12 electronic transitions have been located and assigned. The luminescence from both compounds is weak due to competing nonradiative processes, and the major differences from that of UO_2^{2+} at centrosymmetric sites arise from the electric dipole intensity enhancement of the zero-phonon line and the appearance of progressions in the uranyl antisymmetric stretching mode. Water and hypophosphite modes are identified in the luminescence of **1** and **2**, respectively. The anharmonicities of uranyl stretching modes in **1** are compared with those in other uranyl systems. The Franck−Condon analysis of the absorption and emission spectra of **1** show a U−O bond length increase of 5 ± 1 pm on excitation from σ_u^2 to $\sigma_u\delta_u$, compared with values ranging from 4 to 9 pm for other uranyl systems.

Introduction

In 1992 we synthesized and characterized the new uranium(IV) compound $U(H_2PO_2)_4$.[2] The edges of the dark green plates obtained were found to corrode to a paler yellow color after a period of storage in moist air for several years, indicating oxidation to uranium(VI) as the uranyl ion. We therefore decided to synthesize and characterize uranyl hypophosphite, and during the course of this work we prepared its monohydrate and 1:1 adduct with hypophosphorous acid. Although the crystal systems of these two compounds are monoclinic and orthorhombic, respectively, the uranyl ion is situated at a general position in both. Since the electronic structure of the uranyl ion has been rationalized from spectral measurements using high-symmetry compounds,[3] the comparison with high-resolution spectral data from low-symmetry systems is of interest. Electronic transitions of the uranyl ion which are silent in environments of high symmetry may acquire electric dipole intensity via the odd-parity crystal field operators and become prominent when UO_2^{2+} is situated at a low-symmetry site. The present systems therefore provide the opportunity to investigate whether some excited states are missing from the energy level scheme of Denning.

The free hypophosphite (phosphinate, or dihydrodioxophosphate(I)) anion is best represented by the dipolar structure $H_2P^+-(O^-)_2$ with C_{2v} symmetry.[4] In the solid-state hypophosphite complexes that we have previously investigated,[5] the anion does not coordinate in a bidentate manner to one metal center, but forms a bridge between two centers via one or two of the hypophosphite oxygens. The preparation of (anhydrous) $UO_2(H_2PO_2)_2$ is cited in ref 6 from the precipitation of a uranyl solution by the addition of NaH_2PO_2. We are unaware of previous studies of adducts with hypophosphorous acid, but the crystal structure of the adduct of urea with phosphoric acid has been reported[7] and is of interest because of short, almost symmetrical hydrogen bonds linking these two molecules.

Experimental Section

Synthesis of Compounds. Uranyl hypophosphite monohydrate, $UO_2(H_2PO_2)_2 \cdot H_2O$ (**1**), was prepared by dissolving 5 g (0.01 mol) of $UO_2(NO_3)_2 \cdot 6H_2O$ (Reidel-de-Haën, Reag. ACS) in 30 cm^3 of double-distilled deionized (3D) water in a 100 cm^3 beaker. Between 5 and 20 cm^3 of 50% H_3PO_2 (Reidel-de-Haën, RG) was added to the solution with vigorous stirring. Heat was evolved on mixing, with the formation of a yellow chewing-gum-like substance which became harder with heating and stirring. The solid was broken up with a glass rod into a yellow powder, washed with water, then dissolved in 37% HCl (Reidel-de-Haën), and left for crystals to form, which were subsequently washed

(1) (a) City University of Hong Kong. (b) The Chinese University of Hong Kong.
(2) Tanner, P. A.; Sze, T.-H.; Mak, T. C.; Yip, W.-H. *J. Crystallogr. Spectrosc. Res.* **1992**, *22*, 25.
(3) Denning, R. G. *Struct. Bonding* **1992**, *79*, 215.
(4) Streitweiser, A.; Rajca, A.; McDowell, R. S.; Glaser, R. *J. Am. Chem. Soc.* **1987**, *109*, 4184.
(5) Part 1 of this series: Tanner, P. A.; Faucher, M. D.; Mak, T. C. W. *Inorg. Chem.* **1999**, *38*, 6008.
(6) Seaborg, G. T., Katz, J. J., Eds. *The Actinide Elements*; McGraw-Hill: New York, 1964; p 174.
(7) Ilczyszyn, M. M.; Ratajczak, H.; Barnes, A. J. *J. Raman Spectrosc.* **1992**, *23*, 1.

10.1021/ic990188r CCC: $18.00
Published on Web 11/25/1999

Table 1. Crystallographic Data for $UO_2(H_2PO_2)_2 \cdot H_2O$ and $UO_2(H_2PO_2)_2 \cdot H_3PO_2$

	1	**2**
molecular formula	$UO_2(H_2PO_2)_2 \cdot H_2O$	$UO_2(H_2PO_2)_2 \cdot H_3PO_2$
fw	418.0	466.0
space group	$P2_1/n$ (No. 14)	$P2_12_12_1$ (No. 19)
a (Å)	7.686(2)	7.1572(4)
b (Å)	9.275(2)	7.2363(6)
c (Å)	11.027(2)	17.554(2)
α (deg)	90	90
β (deg)	92.32(3)	90
γ (deg)	90	90
V (Å^3)	785.4(6)	901.0(5)
Z	4	4
calcd dens (g cm^{-3})	3.535	3.435
Mo Kα radiation, λ (Å)	0.710 73	0.710 73
abs coeff (cm^{-1})	210.6	183.9
R_F[a]	0.050	0.036
R_w[b]	0.065	0.042

[a] $R_F = \sum||F_o| - |F_c||/\sum|F_o|$. [b] $R_w = [\sum w(|F_o| - |F_c|)^2/\sum|F_o|^2]^{0.5}$.

and air-dried. Uranium and phosphorus were analyzed by Perkin-Elmer 1000 ICP-AES; hydrogen by Leco CHN-900 analyzer; and H_2O by loss in mass at 105 °C.

Percent by mass found (calcd) for $UP_2O_7H_6$: U 56.67 ± 0.48 (56.94); P 14.49 ± 0.14 (14.82); H 1.394 ± 0.013 (1.447); H_2O 4.6 ± 0.2 (4.3). The compound is insoluble in water and decomposes to a gray-green color on heating to 400 °C.

Uranyl hypophosphite−hypophosphorous acid adduct, $UO_2(H_2PO_2)_2 \cdot H_3PO_2$ (**2**), was prepared by dissolving 5 g (0.01 mol) of $UO_2(NO_3)_2 \cdot 6H_2O$ in 10 cm^3 of 3D water, to which a solution of $NaH_2PO_2 \cdot H_2O$ (1.761 g, 0.02 mol) was added. On mixing, a yellow chewing-gum-like substance appeared, which became hard on heating and stirring. It was broken up into a powder, filtered, washed with water, then dissolved in 50% H_3PO_2, and left in a refrigerator at 4 °C for crystals to form. Energy-dispersive X-ray analysis showed the presence of P and U (in the mole ratio 1.9 ± 0.4 respectively), but no other elements heavier than O.

Percent by mass found (calcd) for $UO_8P_3H_7$: U 50.82 ± 0.93 (51.08); P 19.86 ± 0.25 (19.94); H 1.421 ± 0.007 (1.514). The compound is insoluble in water.

X-ray Data Collection. Crystallographic data for compounds **1** and **2** are summarized in Table 1. Intensities were collected in the variable ω-scan mode on a Rigaku AFC7 diffractometer using Mo Kα radiation (λ = 0.710 73 Å) from a Rigaku rotating-anode generator operated at 50 kV and 90 mA. Empirical absorption correction based on ψ-scan data was applied.

Direct methods yielded the positions of all non-hydrogen atoms. The H atoms of the hypophosphite ions were generated in their idealized positions with P−H bond distances fixed at 1.43 Å and allowed to ride on their parent P atoms. The H atoms of the aqua ligand in **1** and the hydroxy H atom of the hypophosphorous acid molecule in **2** were located in chemically reasonable positions. In each structure the U, P, and O atoms were subjected to full-matrix least-squares anisotropic refinement, and the H atoms were assigned appropriate isotropic temperature factors and included in structure factor calculations.

All calculations were performed on a PC 486 computer with the SHELXTL-PLUS program package.[8] Analytic expressions of atomic scattering factors were employed, and anomalous dispersion corrections were incorporated. The final R indices (refined on $|F|$) are given in Table 1. The final atomic coordinates and thermal parameters are listed in Table 2. Selected bond lengths and bond angles are given in Table 3.

Spectroscopic Measurements. Infrared spectra were recorded from fluorolube and Nujol mulls at a resolution of 2 cm^{-1} using Bomem MB-120 (4000−400 cm^{-1}) and Perkin-Elmer PE-1650 (4000−250 cm^{-1}) spectrometers. Raman and emission spectra were recorded at this same resolution using argon ion laser lines and a Spex 1403-DM spectrometer. The sample was housed in an Oxford Instruments closed-cycle cooler cryostat, with a base temperature of 10 K. A Biorad FTS-60A spectrometer with a Hamamatsu R446 photomultiplier detector was used to record electronic absorption spectra with Nujol mulls or pressed disks. The instruments were calibrated in vacuum wavenumbers using lines from Ne, Hg, and Cd lamps.

(8) Sheldrick, G. M. In *Computational Crystallography*; Sayre D., Ed.; Oxford University Press: New York, 1982; pp 506−514.

Table 2. Selected Bond Lengths (Å) and Angles (deg) for $UO_2(H_2PO_2)_2 \cdot H_2O$ and $UO_2(H_2PO_2)_2 \cdot H_3PO_2$

$UO_2(H_2PO_2)_2 \cdot H_2O$ (**1**)

U(1)−O(1)	1.79(1)	U(1)−O(2)	1.79(1)
U(1)−O(12)	2.36(1)	U(1)−O(21)	2.33(1)
U(1)−O(1W)	2.53(1)	U(1)−O(11a)	2.34(1)
U(1)−O(22b)	2.29(1)	P(1)−O(11)	1.51(1)
P(1)−O(12)	1.52(1)	P(2)−O(21)	1.51(2)
P(2)−O(22)	1.48(2)		
O(1)−U(1)−O(2)	180.0(8)	O(1)−U(1)−O(12)	87.5(5)
O(1)−U(1)−O(21)	90.6(6)	O(1)−U(1)−O(22b)	92.5(6)
O(1)−U(1)−O(1W)	88.1(5)	O(1)−U(1)−O(11a)	92.6(5)
O(21)−U(1)−O(22b)	76.7(5)	O(22b)−U(1)−O(1W)	69.4(5)
O(1W)−U(1)−O(11a)	68.0(4)	O(11a)−U(1)−O(12)	73.8(4)
O(12)−U(1)−O(21)	72.5(5)	P(1)−O(12)−U(1)	132.8(8)
P(1a)−O(11a)−U(1)	141.9(8)	P(2)−O(21)−U(1)	139.1(9)
P(2b)−O(22b)−U(1)	155.9(10)	O(11)−P(1)−O(12)	114.8(8)
O(21)−P(2)−O(22)	115.0(9)		

$UO_2(H_2PO)_2 \cdot H_3PO_2$ (**2**)

U(1)−O(1)	1.78(1)	U(1)−O(2)	1.78(1)
U(1)−O(3)	2.44(1)	U(1)−O(5)	2.36(1)
U(1)−O(6a)	2.42(1)	U(1)−O(7)	2.35(1)
U(1)−O(8b)	2.35(1)	P(1)−O(3)	1.46(1)
P(1)−O(4)	1.51(1)	P(2)−O(5)	1.47(1)
P(2)−O(6)	1.52(1)	P(3)−O(7)	1.49(1)
P(3)−O(8)	1.50(1)		
O(1)−U(1)−O(2)	178.6(5)	O(1)−U(1)−O(3)	90.7(5)
O(1)−U(1)−O(5)	89.2(4)	O(1)−U(1)−O(6a)	92.1(4)
O(1)−U(1)−O(7)	87.8(4)	O(1)−U(1)−O(8b)	91.8(4)
O(3)−U(1)−O(5)	71.2(4)	O(5)−U(1)−O(6a)	71.1(4)
O(6a)−U(1)−O(7)	72.0(4)	O(7)−U(1)−O(8b)	74.1(4)
O(8b)−U(1)−O(3)	71.9(4)	P(1)−O(3)−U(1)	148.0(8)
P(2)−O(5)−U(1)	163.7(7)	P(3)−O(7)−U(1)	143.6(6)
P(2a)−O(6a)−U(1)	127.6(6)	P(3b)−O(8b)−U(1)	135.6(7)
O(3)−P(1)−O(4)	113.5(8)	O(5)−P(2)−O(6)	116.8(6)
O(7)−P(3)−O(8)	116.2(6)		

Results and Discussion

Description of Crystal Structures. In the crystal structure of **1**, the uranium atom has the expected 7-coordinate, pentagonal bipyramidal coordination geometry (Figure 1) that commonly occurs in uranyl salts. The uranyl group is exactly linear with an average U−O bond distance of 1.79(1) Å, and the equatorial coordination sites are occupied by oxygen atoms of four neighboring hypophosphite ions and an aqua ligand in a nearly planar configuration (sum of five equatorial O−U−O bond angles = 360.40°). The U−O (hypophosphite) bond distances lie in the range 2.29−2.36(1) Å, and average to 2.33(1) Å, which is significantly shorter than the U−O(aqua) bond distance of 2.53(1) Å.

As shown in Figure 1, both independent hypophosphite ions take turns in serving as bridging ligands between pairs of uranium atoms along a polymeric chain, which comprises an alternate arrangement of corner-sharing, centrosymmetric, doubly bridged eight-membered rings with uranium atoms at the ring junctions. Parallel chains in the [$\bar{1}$10] direction lie near the plane $z = 0$. The n-glide operation generates an equivalent planar array of chains directed along [110] at $z = {}^1/_2$, and the crystal structure is built of alternate layers of differently oriented polymeric chains (Figure 2).

The coordination geometry about the uranium atom in compound **2** (Figure 3) is similar to that in **1**. The uranyl group

Table 3. Atomic Coordinates ($\times 10^5$ for U; $\times 10^4$ for Other Atoms) and Equivalent Isotropic Temperature Factors[a] (Å^2 $\times$ 10^4 for U; $\times 10^3$ for Other Atoms) for $UO_2(H_2PO_2)_2 \cdot H_2O$ (**1**) and $UO_2(H_2PO_2)_2 \cdot H_3PO_2$ (**2**)

atom	*x*	*y*	*z*	U_{eq}/U_{iso}
		Compound **1**		
uranyl group				
U(1)	28142(9)	23447(6)	55674(6)	198(2)
O(1)	1566(18)	3210(14)	6693(11)	31(4)
O(2)	4061(18)	1484(15)	4445(12)	34(4)
hypophosphite ions				
P(1)	−1511(6)	1437(4)	4517(4)	22(1)
H(1A)	−1843	1426	5784	60
H(1B)	−2856	2271	3919	60
O(11)	−1605(18)	−87(14)	4039(12)	32(4)
O(12)	221(19)	2196(13)	4350(12)	29(4)
P(2)	3683(9)	5149(6)	3415(5)	43(2)
H(2A)	2476	5630	2480	60
H(2B)	4844	4151	2879	60
O(21)	2653(19)	4406(16)	4362(14)	41(5)
O(22)	4710(22)	6413(15)	3857(15)	46(5)
aqua ligand				
O(1W)	4468(19)	1042(13)	7270(13)	32(4)
H(1WA)	4167	194	7586	60
H(1WB)	4716	1601	7922	60
		Compound **2**		
uranyl group				
U(1)	19698(6)	2145(6)	37756(3)	239(1)
O(1)	2879(16)	−1694(14)	3259(6)	39(3)
O(2)	1041(15)	2086(13)	4310(6)	33(3)
hypophosphorous acid molecule				
P(1)	6327(5)	3097(5)	3731(2)	33(1)
H(1A)	7771	3003	3169	80
H(1B)	7026	2261	4412	80
O(3)	4718(16)	2050(17)	3462(7)	55(4)
O(4)	5898(23)	5104(15)	3889(6)	68(5)
H(4)	5838	5663	4351	80
hypophosphite ions				
P(2)	5580(5)	−1131(5)	5255(2)	31(1)
H(2A)	5087	−549	6007	80
H(2B)	7405	−421	5098	80
O(5)	4267(16)	−276(15)	4718(6)	48(3)
O(6)	5695(17)	−3226(13)	5249(6)	36(3)
P(3)	−2106(6)	−1446(5)	2728(2)	32(1)
H(3A)	−2242	−20	2166	80
H(3B)	−3960	−1846	2983	80
O(7)	−1019(13)	−718(14)	3386(5)	34(3)
O(8)	−1344(17)	−3149(16)	2352(6)	47(4)

[a] For U, P, and O atoms, U_{eq} is defined as one-third of the trace of the orthogonalized **U** tensor. For H atoms the exponent takes the form $-8\pi^2 U_{iso} \sin^2 \theta/\lambda^2$.

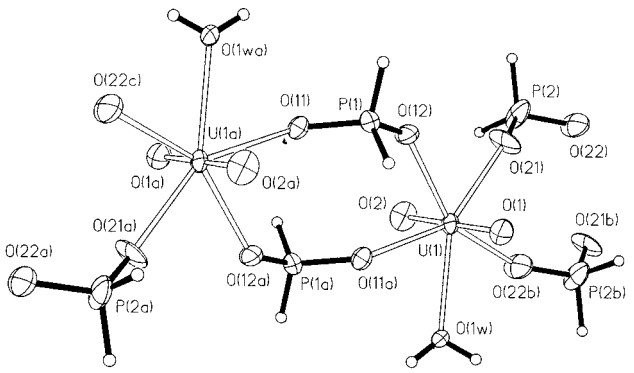

Figure 1. Coordination environment of the uranium atom in $UO_2(H_2PO_2)_2 \cdot H_2O$ (**1**) and the atom-numbering scheme. The thermal ellipsoids are drawn at the 50% probability level. Symmetry codes: a $(-x, -y, 1 - z)$; b $(1 - x, 1 - y, 1 - z)$.

is nearly linear with O−U−O = 178.6(5)° and an average U−O bond length of 1.78(1) Å. The equatorial oxygen ligand atoms

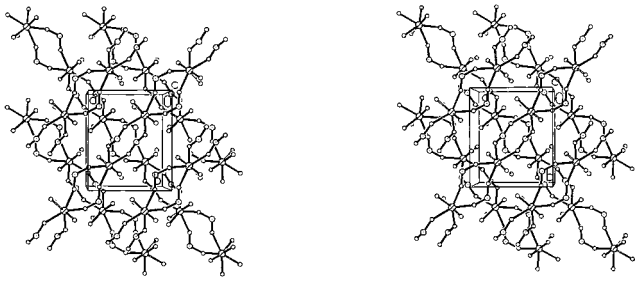

Figure 2. Stereoview of the crystal structure of **1** showing two successive layers of parallel polymeric chains stacked normal to the *c* axis. Note the crisscross relationship between the chains lying in different layers.

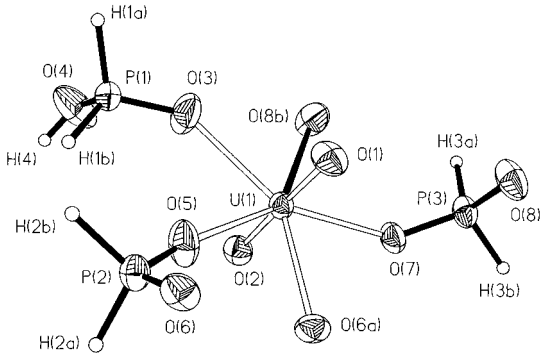

Figure 3. Coordination environment of the uranium atom in $UO_2(H_2PO_2)_2 \cdot H_3PO_2$ (**2**) and the atom-numbering scheme. The thermal ellipsoids are drawn at the 50% probability level. Symmetry codes: a $(-{}^1/_2 + x, -{}^1/_2 - y, 1 - z)$; b $(-x, {}^1/_2 + y, {}^1/_2 - z)$.

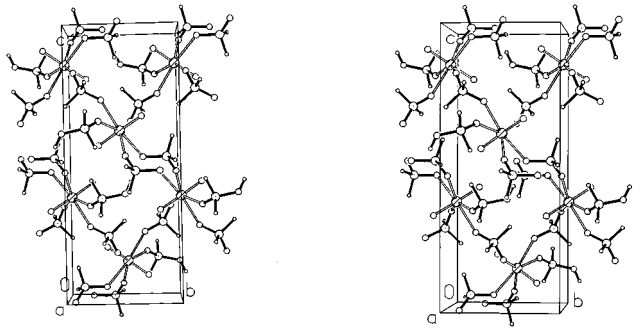

Figure 4. Stereoview of the crystal structure of **2** showing the three-dimensional coordination network constructed from the bridging hypophosphite ions. The origin of the unit cell lies at the lower left corner, with *a* pointing toward the reader, *b* from left to right, and *c* upward.

are virtually coplanar (sum of O−U−O bond angles = 360.30°), and the U−O bond lengths lie in the range 2.35−2.44(1) Å.

Although the neutral hypophosphorous acid molecule cannot be clearly distinguished from the two independent hypophosphite ions on the basis of measured P−O bond lengths, its identity can be ascertained by the fact that it functions only as a unidentate terminal ligand, whereas the hypophosphite ions serve as bridging ligands. However, unlike the case for **1**, the hypophosphites in **2** each *singly* bridge a pair of neighboring uranium ions, resulting in a three-dimensional coordination network structure as illustrated in Figure 4.

Although in both **1** and **2** the uranium atom is situated in a pentagonal bipyramidal arrangement as in $UO_2(O_3PCH_2Cl)$ and $UO_2(HOCH_2PO_3) \cdot 5H_2O$,[9] the latter structures differ in that

(9) Poojary, D. M.; Grohol, D.; Clearfield, A. *J. Phys. Chem. Solids* **1995**, *56*, 1383.

$UO_2(O_3PCH_2Cl)$ has two-dimensional layers and $UO_2(HOCH_2PO_3)\cdot 5H_2O$ has hydrogen-bonded chains of isolated uranyl polyhedra.

Infrared and Raman Spectra. The spectra of **1** comprise characteristic vibrations of water, the uranyl ion, and the hypophosphite ion. The vibrational couplings between the water molecules in the unit cell are weak and do not produce resolvable infrared band splittings. The isolated $H_2PO_2^-$ ion has nine modes of vibration, all of which are nondegenerate:

$$\Gamma(\text{vib: } C_{2v}) \in \{\nu_1,\nu_2,\nu_3,\nu_4(\alpha_1);\nu_5(\alpha_2);\nu_6,\nu_7(\beta_1);\nu_8,\nu_9(\beta_2)\} \quad (1)$$

The normal vibrations have been previously firmly assigned from polarized infrared and Raman spectra of the anion and its deutero analogue (refs 10,11 and references therein). The more recent reassignments[12] are in error and have been discussed elsewhere.[13] In the solid state, unit cell group (factor group) vibrational couplings occur between $H_2PO_2^-$ ions, which give rise to multiple spectral structure for each parent ion normal mode of vibration. In favorable cases, such as in $Ln(H_2PO_2)_3$,[5] the individual unit cell group modes may be resolved in the vibrational spectra. For **1**, with two sets of four $H_2PO_2^-$ ions, each occupying C_1 sites in the Bravais cell, each hypophosphite mode should give rise to four IR-active $[2\alpha_u+2\beta_u(C_{2h})]$ and four (noncoincident) Raman-active $[2\alpha_g+2\beta_g(C_{2h})]$ unit cell group modes. The hypophosphite modes in the infrared and Raman spectra of **1** are assigned in Table 4 by associating the parent ion mode with the unit cell group components. In congested spectral regions, such as between 1000 and 1300 cm^{-1}, the assignments are not clear-cut. Four components are resolved in the higher energy region of the infrared spectrum of **1** between 2391 and 2450 cm^{-1} (Table 4, Figure 5c) for the two P−H stretching modes. In the corresponding region of the Raman spectrum, Figure 5a, four features are also resolved, and only one of these is coincident with an infrared band. The situation is more complex in **2**, with two sets of four $H_2PO_2^-$ ions each at C_1 sites in the Bravais cell. In this case each parent hypophosphite ion mode may give rise to six infrared $[2\beta_1+2\beta_2+2\beta_3(D_2)]$ and eight Raman $[2\alpha+2\beta_1+2\beta_2+2\beta_3(D_2)]$ bands, with some coincidences, but coupling of these modes with the appropriate vibrations of the four H_3PO_2 molecules at C_1 sites in the unit cell will further complicate the vibrational spectra. At least five infrared bands (Figure 5d) and five Raman bands (Figure 5b) are resolved in the P−H stretching region. Some unique bands in the spectrum of **2** clearly indicate the presence of the hypophosphorous acid molecule, and these are labeled in Table 4 together with the wavenumbers in solid H_3PO_2, by the notation of Lovejoy and Wagner,[14] who studied the infrared spectrum of H_3PO_2 at −180 °C. The phosphorus−oxygen modes of H_3PO_2 differ from those of $H_2PO_2^-$, and the P−O stretch and O═P−OH scissor deformation are observed with medium intensity in the infrared spectrum of **2** at 966 and 419 cm^{-1}, indicating a slightly stronger P−O bond in the complexed acid in **2** rather than the (hydrogen-bonded) acid anion. The P−H stretch region in the infrared spectrum of the free acid H_3PO_2 is poorly resolved,[14] and the weak, broad O−H stretch reported at 2700 cm^{-1} is characteristic of hydrogen-bonded systems. The O−H stretching mode is not prominent in the infrared spectrum of **2**. At room temperature a very weak broad feature is observed, centered near 2890 cm^{-1}, with a further weak band at 3475 cm^{-1}. Without deuteration studies it is not possible to distinguish the assignments of these bands to fundamental or combination modes.

The most distinguishing features in the vibrational spectra of uranyl compounds are the bands due to the symmetric and antisymmetric O−U−O stretching modes, labeled $\nu_1\nu_s$(OUO) and $\nu_2\nu_{as}$(OUO) hereafter, which are Raman and infrared active, respectively, for an isolated, centrosymmetric uranyl ion. The electronic ground-state vibrational energies of these modes change according to the nature of the ligand and the coordination

Table 4. Vibrational Spectra of $UO_2(H_2PO_2)_2\cdot H_2O$ and $UO_2(H_2PO_2)_2\cdot H_3PO_2$

wavenumber (cm^{-1})				
$UO_2(H_2PO_2)_2\cdot H_2O$		$UO_2(H_2PO_2)_2\cdot H_3PO_2$		
IR[a]	Raman[b]	IR[a]	Raman[b]	assignment[c]
3514m				$\nu_{as}(H_2O)$
3322w				$\nu_s(H_2O)$
3183w				$2\delta(H_2O)$
2448w	2459s	2480w	2482m	$\nu_1\nu_s(PH_2)$
2414m	2424s	2457m	2462s	
2400m	2406m	2420ms	2426m	
		2407s	2412ms	
2391s	2391s	2394ms	2396s	$\nu_6\nu_{as}(PH_2)$
		2346w		2319, $\nu_s(PH_2)$
1736vw				ν_s(OUO) + ν_{as}(OUO)
1619m				$\delta(H_2O)$
1196w				$\nu_8\nu_{as}(PO_2)$
1184w				
		1178w	1196mw	1184, ν(P═O)
1168sh	1152m	1163sh	1159sh	
1145s	1142m	1148s	1148ms	$\nu_2\delta_{scissor}(PH_2)$
		1140sh	1140m	
(1133sh)	1128m	1134s		1124, $\delta_{scissor}(PH_2)$
1122s	1104m	1119ms	1124sh	$\nu_9\delta_{wag}(PH_2)$
		1114m	1116s	
1082m	1081sh	1092sh	1096mw	
1073s	1074ms	1086m	1082m	$\nu_3\nu_s(PO_2)$
1066sh	1062m	1073ms	1066ms	1055, $\delta_{wag}(PH_2)$
			1056m	
1039m	1038m	1032ms	1042s	
		1023ms	1032sh	
			1008m	
		966ms	964mw	950, ν(P−O)
		935vw	940s	−, $\delta_{twist}(PH_2)$
919m	918ms	918sh		$\nu_5\delta_{twist}(PH_2)$
909s	910ms	912s		ν_{as}(OUO)
832w	830s	834m	830s	ν_s(OUO)
814ms	822m	813sh	814m	$\nu_7\delta_{rock}(PH_2)$
807sh	810m	810ms	802mw	
802sh		799m		803, $\delta_{rock}(PH_2)$
(668w)	684vw			
566bm	572vw			libr (H_2O)
483mw	496w	497m	502mw	$\nu_4\delta_{scissor}(PO_2)$
460m	484w	489m	490m	
		481sh	482m	
		419m	416mw	428, $\delta_{scissor}$(O═P−OH)
336w	328vw			ν_{as}(U−O)
	302vw			ν_s(U−O)
285w	278vw			δ(OUO)
280w	266m			
270s	253vw			
	240mw			
	220ms			δ_{rock}(OUO)
209s	210sh			
	(158)			

[a] Room temperature. [b] 80 K. [c] The infrared wavenumbers and mode description for H_3PO_2 are from ref 14.

(10) Tanner, P. A.; Sze, T.-H.; Mak, T. C. W.; Wang, R.-J. *Polyhedron* **1992**, *11*, 817.
(11) Tanner, P. A.; Liu, Y.-L.; Mak, T. C. W. *Polyhedron* **1997**, *16*, 495.
(12) Bickley, R. I.; Edwards, H. G. M.; Knowles, A.; Tait, K. F.; Gustar, R. E.; Mihara, D.; Rose, S. J. *Spectrochim. Acta* **1994**, *50A*, 1277.
(13) Liu, R.; Moody, P. R.; Vanburen, A. S.; Clark, J. A.; Krauser, J. A.; Tate, D. R. *Vibrational Spectrosc.* **1996**, *10*, 325.
(14) Lovejoy, R. W.; Wagner, E. L. *J. Phys. Chem.* **1964**, *68*, 544.

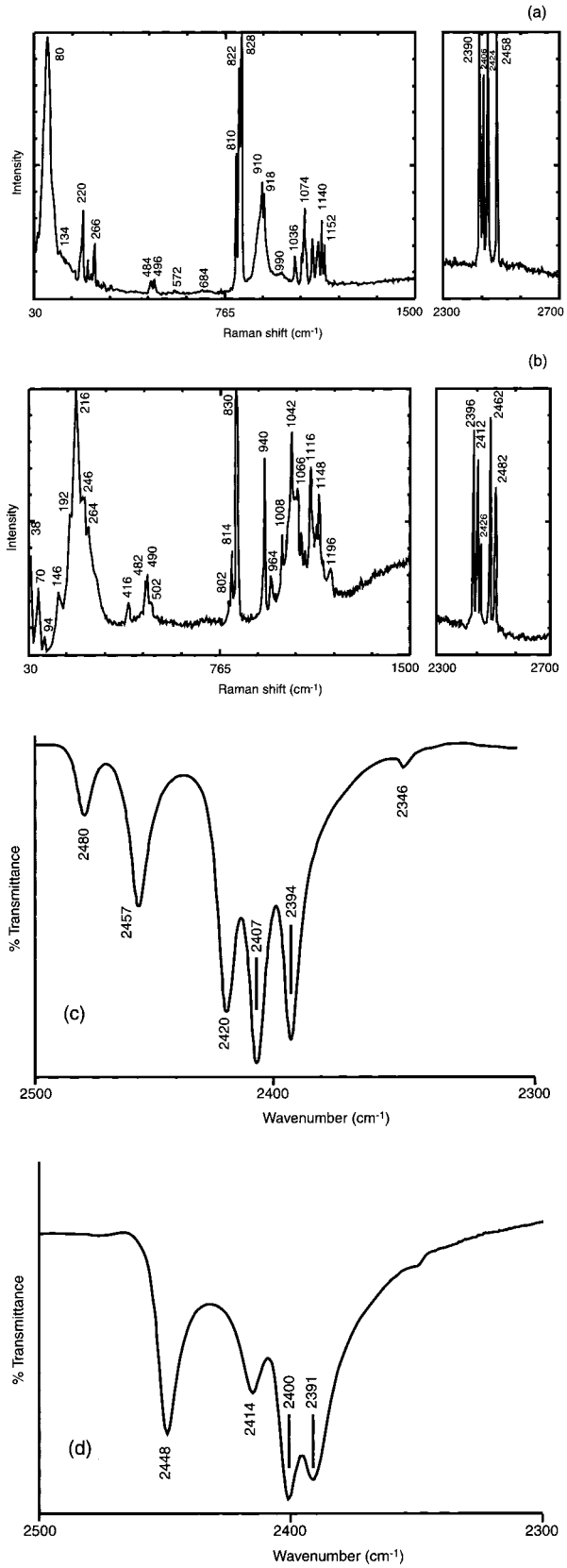

Figure 5. 514.5 nm excited 80 K Raman spectra of (a) $UO_2(H_2PO_2)_2 \cdot H_2O$ and (b) $UO_2(H_2PO_2)_2 \cdot H_3PO_2$ between 30 and 1500 cm^{-1} and 2250 and 2700 cm^{-1}; and P−H stretch region of the 300 K infrared absorption spectrum of (c) $UO_2(H_2PO_2)_2 \cdot H_2O$ and (d) $UO_2(H_2PO_2)_2 \cdot H_3PO_2$ between 2300 and 2500 cm^{-1}. Broad features near 80 and 910 cm^{-1} in panel a are due to uranyl emission.

geometry of the uranyl ion, but also the modes are at higher energies in uranyl compounds which have smaller counter-cations.[15−18] Environments with lower equatorial charge surrounding the uranyl ion produce a shorter U−O bond distance and, hence, a higher $\nu_1\nu_s$(OUO) stretching frequency. This is the case with smaller equatorial coordination number (e.g., $[Me_4N]_2UO_2F_4$ 801 cm^{-1} versus $Cs_3UO_2F_5$ 783 cm^{-1}), more polarizing counterions (e.g., $Li_2UO_2Cl_4$ 869 cm^{-1} versus $Cs_2UO_2Cl_4$ 836 cm^{-1}), or more polarizable ligands (e.g., $[Me_4N]_2UO_2Br_4$ 834 cm^{-1} versus $[Me_4N]_2UO_2Cl_4$ 829 cm^{-1} and $[Me_4N]_2UO_2F_4$ 801 cm^{-1}). More highly charged equatorial environments, as for octahedrally coordinated uranium in uranates, give rise to lower ν_s(OUO) energies, 730 cm^{-1} in the case of Ba_2CaUO_6,[19] because the uranium 5f−oxygen 2p bonding interaction is destabilized relative to uranium 6p−oxygen 2p antibonding interaction.[3] The energy of the most intense Raman-active symmetric stretching mode ν_s(OUO) in **1** and **2** is 830 cm^{-1}, from which the U−O bond distance, R_{U-O} (in Å) in the electronic ground state is estimated by the regression of Bartlett and Cooney,[20]

$$R_{U-O} = 106.5(\bar{\nu}_1)^{-2/3} + 0.575 \qquad (2)$$

to be 1.78 Å, in good agreement with the X-ray results. For **1**, two infrared-active $[A_u+B_u(C_{2h})]$ and two noncoincident Raman-active $[A_g+B_g(C_{2h})]$ unit cell group modes are derived for each of the ν_{as}(OUO) and ν_s(OUO) vibrations, from the unit cell group analysis, whereas four Raman and three infrared bands are expected for **2**. The couplings between symmetric stretching modes of different uranyl ions in the unit cell are weak, whereas the long-range dipole coupling is greater for the ν_{as}(OUO) mode. Two bands are resolved in the infrared spectrum near 910 cm^{-1} for both **1** and **2**, but the weaker component may otherwise arise from the PH_2 twist.

Emission Spectra of Uranyl Hypophosphites. The electronic ground state of the $D_{\infty h}$ symmetry uranyl ion is $^1\Sigma_g^+$, with the first excited electronic state being the degenerate $^1\Pi_g$ state. Generally, this excited-state energy increases together with ν_s(OUO), due to a strengthening of σ_u bonding interaction, and is expected to be near 20 000 cm^{-1} when the energy of this vibration is about 830 cm^{-1}.

The luminescence from **2** is weak because coupling of the Π_g excited state to the high energy P−H and O−H stretching modes provides a competitive nonradiative relaxation process. However, the luminescence from **1** is even weaker because of nonradiative relaxation via six quanta of $\nu(OH_2)$ from H_2O in the first coordination sphere. The 80 K luminescence spectrum of **1**, when excited by 476.5 or 488 nm argon ion laser radiation, contains a broad intense trap band to slightly lower energy than the position of the absorption spectrum zero-phonon line. The emission spectrum differs from that of the uranyl ion at a centrosymmetric site[16] in several respects, although the Franck−Condon maximum intensity is also at $v = 1$. First, the strongest features correspond to the progression in $n\nu_1\nu_s$(OUO) upon the zero-phonon line, because the electronic transition gains electric dipole character at the C_1 uranium site due to static mixing of 6d and 5f orbital states via the crystal field. Second, progressions in $n\nu_2\nu_{as}$(OUO) may be followed to $n = 3$, since this mode is

(15) Flint, C. D.; Tanner, P. A. *Mol. Phys.* **1981**, *43*, 933.
(16) Flint, C. D.; Tanner, P. A. *J. Chem. Soc., Faraday Trans. 2* **1981**, *77*, 1865.
(17) Flint, C. D.; Tanner, P. A. *J. Chem. Soc., Faraday Trans. 2* **1982**, *78*, 103.
(18) Flint, C. D.; Tanner, P. A. *J. Chem. Soc., Faraday Trans. 2* **1984**, *80*, 219.
(19) Krol, D. M.; Blasse, G. *J. Chem. Phys.* **1978**, *69*, 3124.
(20) Bartlett, J. R.; Cooney, R. P. *J. Mol. Struct.* **1989**, *193*, 295.

Table 5. Anharmonicity Constants, x_{ii} and x_{ij}, and Harmonic Frequencies, $\bar{\nu}_1^h$ (All in cm^{-1}), in the Σ_g^+ State for Selected Uranyl Compounds

compd	x_{11}	x_{12}	x_{22}	$\bar{\nu}_1^h = \bar{\nu}_1 - 2x_{11} - 0.5x_{12}$
$UO_2(H_2PO_2)_2 \cdot H_2O$ (**1**)	−2.1	−7.1	−1.8	838
$Cs_2UO_2Cl_4$[21]	−1.5	−6.0		838
$[(C_2H_5)_3NH]_2UO_2Cl_4$[22]	−1.5	−6.4		841
$K_3UO_2F_5$[15]	−1.5	−5.7		812
$K_5(UO_2)_2F_9$[23]	−1.1	−5.3		813
$Cs_2(UO_2)_2F_6(OH_2)_2$[23]	−1.5	−5.4		823

totally symmetric at the uranium site in the present case. The vibronic origins are relatively weaker, compared with the above progressions, than in the spectra of centrosymmetric uranyl ions, such as $[(CH_3)_4N]_2UO_2Cl_4$.[16] The anharmonicity constants x_{ii} and x_{ij}[21] for $\nu_1\nu_s$(OUO) and $\nu_2\nu_{as}$(OUO) in the electronic ground state were fitted from the separations, $\Delta G(n + {}^1/_2)$, of $(n + 1)\nu_i$ from $n\nu_i$ ($i = 1$ or 2),

$$\Delta G(n + {}^1/_2) = \bar{\nu}_i^h + x_{ii}(2n + 1) \tag{3}$$

and ΔG, of $n\nu_1 + \nu_2$ from $n\nu_1$,

$$\Delta G = \bar{\nu}_2^h + x_{22} + nx_{12} \tag{4}$$

where $\bar{\nu}_i^h$ is the harmonic frequency (cm^{-1}) of mode i. The derived quantities are listed in Table 5, where comparison with values from other uranyl systems shows that $x_{11} \approx x_{22} \approx 1-2$ cm^{-1} and $x_{12} \approx 5-7$ cm^{-1}. The derived energies of ν_2 from the $n\nu_1 + \nu_2$ progression do not show a monotonic decrease with n, however, presumably due to Fermi resonance with $n\nu_1\nu_s$-(OUO) + $\nu_5(PH_2)$, but the 80 K spectra are not sufficiently well-resolved to investigate this further. Weak features at 223, 275, 327, 490, and 579 cm^{-1} below the zero-phonon line are assigned to OUO rock and bend, U−O(eq) antisymmetric stretch, PO_2 scissor, and water libration, respectively. The energy of the U−O(hyp) antisymmetric stretch is rather lower than that of the U−OH_2 stretch in $Cs_2(UO_2)_2F_6(OH_2)_2$ (near 400 cm^{-1}),[23] although the U−O bond distance is similar (2.35 Å), partly because the latter mode is extensively mixed with ν_{as}(U−F). In the low-energy region of the luminescence spectrum, the distinctly different Franck−Condon pattern of some features from nearby bands enables them to be assigned to the members of the $n\nu_1\nu_s$(OUO) + $\nu_{as}(OH_2)$ progression.

The luminescence of **2** is analogously assigned as above and is therefore not described in detail. The most interesting features correspond to a clearly located $n\nu_1\nu_s$(OUO) + ν(PH) progression ($n = 0-4$), with the derived wavenumber of the PH stretching mode maximum being 2410 cm^{-1}. This region of the luminescence spectrum is not as well-resolved as the P−H stretch region of the infrared spectrum, and this energy is near to the mean value of the three $\nu_6\nu_{as}(PH_2)$ infrared-active modes (Table 4).

Electronic Absorption Spectra of Uranyl Hypophosphites. The identifications and locations of the excited states in $Cs_2UO_2Cl_4$ and $CsUO_2(NO_3)_3$, where the UO_2^{2+} site symmetry approaches D_{2h} and D_{3h}, respectively, have been reviewed by Denning.[3] The energy levels of the uranyl ion at a D_{5h} site have been rationalized under this model[15] and may serve as the starting point for comparison with the electronic spectra of uranyl hypophosphites, where UO_2^{2+} has distorted 5-fold in-plane coordination geometry. Figure 6a shows the survey 15 K absorption spectra between 20 000 and 27 000 cm^{-1} for **1** and **2**, with the first group of bands in each case being shown in Figure 6b,c. The analyses of these complex spectra are rather lengthy and involved, and in places ambiguous, but are consistent with previous studies.[15−17,23] The derived energies of the excited states, together with the OUO symmetric stretch progression energies, are listed in Table 6 for comparison with results from $K_3UO_2F_5$. Not all of the site-symmetry splittings of electronic states are resolved in the fairly broad bands of these spectra, but there is no clear evidence, in the spectral

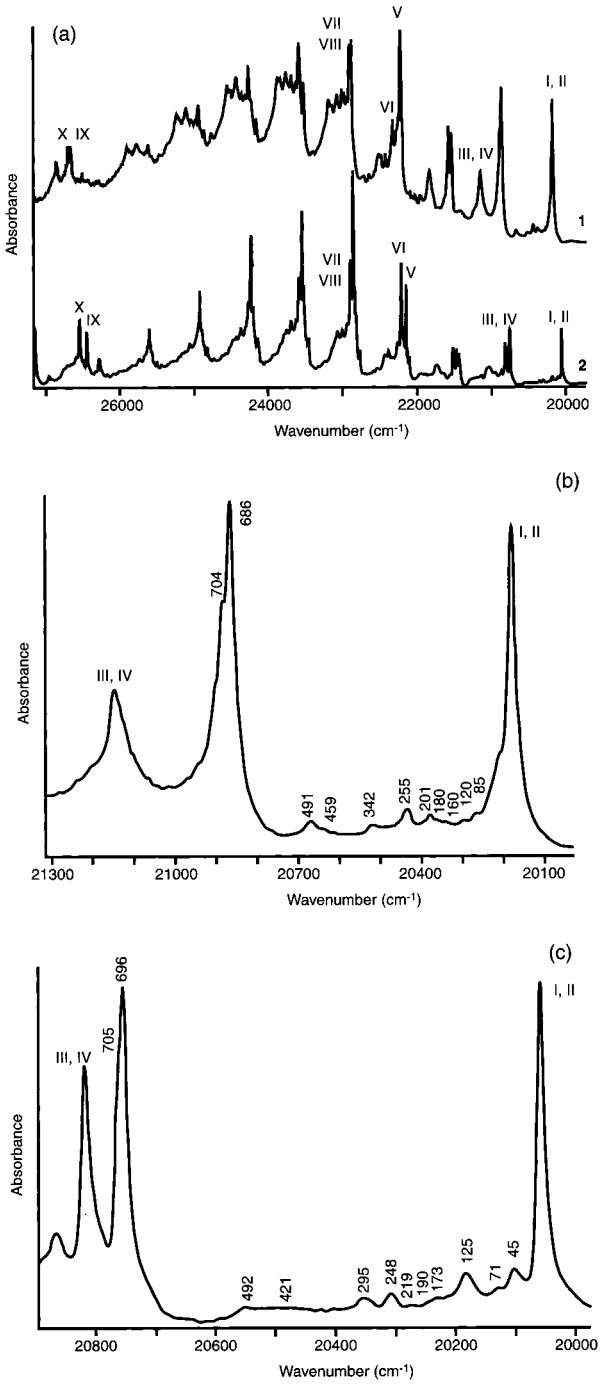

Figure 6. (a) Survey 15 K absorption spectra of **1** and **2** between 20 000 and 27 000 cm^{-1}; (b, c) More detail of the first group of bands of **1** and **2**, respectively, with wavenumber intervals above origins I,II marked.

(21) Flint, C. D.; Tanner, P. A. *J. Chem. Soc., Faraday Trans. 2* **1978**, *74*, 2210.
(22) Flint, C. D.; Tanner, P. A. *J. Chem. Soc., Faraday Trans. 2* **1979**, *75*, 1168.
(23) Flint, C. D.; Tanner, P. A. *J. Chem. Soc., Faraday Trans. 2* **1981**, *77*, 2339.

Table 6. Excited Electronic States and $\nu_s\nu_1$(OUO) Progression Energies (in cm^{-1}) Assigned from the 15 K Electronic Absorption Spectra of $UO_2(H_2PO_2)_2 \cdot H_2O$ and $UO_2(H_2PO_2)_2 \cdot H_3PO_2$ between 20 000 and 27 000 cm^{-1}

D_{5h} excited state[a]	energy in $K_3UO_2F_5$	energy (ν_1) in $UO_2(H_2PO_2)_2 \cdot H_2O$ (**1**)	energy (ν_1) in $UO_2(H_2PO_2)_2 \cdot H_3PO_2$ (**2**)
I,II (E_1'')	19 982, 19 987	20 180 (686)	20 059 (696)
III,IV (E_2')	20 970, 20 975	21 148 (680)	20 820 (690)
V,VI (E_2'')		22 224 (687)	22 152 (688)
		22 327 (683)	22 214 (688)
VII,VIII (E_2')		ca. 23 000 (682)	ca. 23 000 (683)
IX,X (E_2'')		26 514 (705)	26 450 (708)
		?	26 546 (707)
XI,XII (E_1')		ca. 28 740	ca. 28 730

[a] Corresponding D_{5h} irreducible representations for the uranyl excited-state scheme of Denning.[3]

region studied, for the location of additional electronic transitions, other than those predicted from the model of Denning. Some features of the assignments are briefly discussed below.

The weak features marked in Figure 6b,c up to 20 700 cm^{-1} correspond to lattice modes, OUO rock and bend, U−O(hyp) stretch, and PO_2 scissor modes based upon electronic origins I,II at 20 180 cm^{-1} in **1** and 20 059 cm^{-1} in **2**. The U−O(hyp) stretch energy is slightly higher (by about 10 cm^{-1}) than in the electronic ground state, which contrasts with the behavior in uranyl fluoride complexes where the U−F stretch decreases by several wavenumbers in the Π_g state. The first member of the ν_1 progression on origins I,II is at 686 cm^{-1} (**1**) (or 696 cm^{-1} (**2**)) to high energy and is just resolved from ν_2 704 cm^{-1} (**1**) (or 705 cm^{-1} (**2**)). A further strong band to slightly higher energy is assigned to one or both of the components of the hypersensitive $\Sigma_g^+ \rightarrow \Delta_g$ transition, with extensive vibronic structure up to 462 cm^{-1} higher energy in the case of **2**. The further complexity near $\Sigma_g^+ \rightarrow \Pi_g + 2\nu_1$ is due to the progression $\Sigma_g^+ \rightarrow \Pi_g + 2\nu_2$. New strong bands in the region near 22 200 cm^{-1} for both **1** and **2** must correspond to further electronic transitions, V,VI, with the most reasonable locations given in Table 6. Further new sharp bands in the region of V,VI + $n\nu_1$ are clearly identified as the anharmonic V,VI + $n\nu_2$ progression. By contrast to the states I,II, the wavenumber of ν_2 is at 20−30 cm^{-1} lower energy than that of ν_1 in these electronic states V,VI. However, some broader bands associated with vibronic structure just above 23 000 cm^{-1} show a different Franck−Condon pattern from structure based on V,VI in **1** and could be associated with a further electronic transition(s). There is no evidence for the observation of high-energy vibrational modes, such as $\nu(OH_2)$ or $\nu(PH_2)$, based on the origins I−IV. Strong bands at 26 450, 26 546 cm^{-1} in **2**, with the ν_1 progression frequency 707 cm^{-1}, correspond to new electronic origins, IX,X. The corresponding region of **1** is more complex, and although a new origin is clearly located at 26 514 cm^{-1}, it is not possible to distinguish vibronic from electronic transitions in the region to slightly higher energy. The energy of ν_2 is again ca. 30 cm^{-1} lower than that of ν_1 for these electronic states IX,X. A further new electronic transition near 28730−28740 cm^{-1} in both **1** and **2** exhibits total absorption in our spectra and corresponds to origin(s) XI,(XII).

Franck−Condon Analysis of Emission and Absorption Spectra. The intensities of the $\Sigma_g^+ + n\nu_1 \leftarrow \Pi_g$ emissive transitions, $I_{n,0}$ ($n = 0$, ..., n vibrational level of Σ_g^+ state; 0 denotes that the transition originates from the zero-point energy level of Π_g), show a maximum for $n = 0$ in salts of the $UO_2Cl_4^{2-}$ ion, but at $n = 1$ for salts of $UO_2F_5^{3-}$ (or $UO_2F_4^{2-}$), where the higher equatorial charge (or less polarizable ligand) leads to lower $\nu_1\nu_s$(OUO) energies. Equatorial U−F bond lengths exhibit a larger change upon the excitation of the electron from the σ_u orbital than U−Cl bond lengths, as shown by the observations of progressions in the totally symmetric ν_s(U−F) mode in luminescence.[15] For the hypophosphites, the Franck−Condon maximum in the $n\nu_1\nu_s$(OUO) progressions in emission is at $n = 0$. Fits to the intensities $I_{n,0}$ ($n = 1$, ..., 4) were utilized to calculate the ratios of overlap integrals:

$$\frac{I_{n,0}}{I_{0,0}} = \left[\frac{E(\mathrm{ZPL}) - n\bar{\nu}_1}{E(\mathrm{ZPL})}\right]^4 \left[\frac{\langle n|0\rangle}{\langle 0|0\rangle}\right]^2 \qquad (5)$$

where E(ZPL) is the zero phonon line energy and $n\nu_1$ is the energy of n quanta of $\nu_1\nu_s$(OUO). This formula neglects the changes in bulk refractivity and effective field correction with energy, which is justifiable in the present case for the change in energy of ca. 3000 cm^{-1} from the green spectral region. The overlap integrals $\langle n|0\rangle$ and $\langle 0|0\rangle$ may also be calculated from recursion formulas[24] involving a dimensionless Franck−Condon offset parameter a_{ge} ($g = \Sigma_g^+$ ground state; e = Π_g excited state) and the angle θ given by

$$\tan\theta = \left[\frac{\bar{\nu}_1\nu_s(\mathrm{OUO})_e}{\bar{\nu}_1\nu_s(\mathrm{OUO})_g}\right]^{0.5} \qquad (6)$$

From the parameter $a_{g,e}$ the Huang−Rhys parameters for the ground (S_g) and excited (S_e) states may be evaluated,

$$S_g = 0.5{a_{ge}}^2 \cos^2\theta \quad \text{and} \quad S_e = 0.5{a_{ge}}^2 \sin^2\theta \qquad (7)$$

and the offset along the α_{1g} coordinate, x (pm), between the ground and excited states can be calculated from S_t (where t = g or e),

$$x = 2^{-1/2}10^{12}\left[\frac{0.5S_t}{\pi^2\bar{\nu}_1}\frac{h}{cM_0}\right]^{0.5} \qquad (8)$$

where h (J s) and c (cm s^{-1}) are constants and M_0 (kg) is the reciprocal of the G-matrix element of the $\nu_1\nu_s$(OUO) normal mode of vibration of the linear triatomic UO_2^{2+}. Note that the factor $2^{-1/2}$ in (eq 8) has been neglected in our previous studies and in other work,[25,26] but it relates the α_{1g} normal coordinate to the change in each U−O bond distance. The various degrees of approximation in Franck−Condon calculations have previously been described elsewhere.[27] In **1** the derived magnitudes of S_g and S_e (0.70 and 0.58, respectively) are found to differ from those reported for Cs_2ZrCl_6:$UO_2Cl_4^{2-}$ (1.05 and 0.89[25]), although the calculated U−O bond length increase, 4 pm, is comparable with those upon excitation in other salts of the uranyl ion, with the (recalculated) values $Cs_2UO_2Cl_4$ 4 pm, $[(C_2H_5)_3NH]_2UO_2Cl_4$ 5 pm, $[(CH_3)_4N]_2UO_2Br_4$ 6 pm, $(NH_4)_3UO_2F_5$ 7 pm, $[(CH_3)_4N]_2UO_2F_4$ 8 pm, and $Cs_3UO_2F_5$ 9 pm, and corrected values $Na[UO_2(CH_3COO)_3]$ 5 pm[26] and Cs_2ZrCl_6:$UO_2Cl_4^{2-}$ 5 pm.[25]

The Franck−Condon analysis of the $\Sigma_g^+ \rightarrow \Pi_g + n\nu_1$ absorption spectrum utilizes the relation 9 instead of 5,

(24) Struck, C. W.; Fonger, W. H. *J. Lumin.* **1975**, *10*, 1.
(25) Metcalf, D. H.; Dai, S.; Del Cul, G. D.; Toth, L. M. *Inorg. Chem.* **1995**, *34*, 5573.
(26) Moran, D. M.; Metcalf, D. H.; Richardson, F. S. *Inorg. Chem.* **1992**, *31*, 819.
(27) Yersin, H.; Otto, H.; Zink, J. I.; Gliemann, G. *J. Am. Chem. Soc.* **1980**, *102*, 951.

$$\frac{I_{0,n}}{I_{0,0}} = \left[\frac{E(\mathrm{ZPL}) + n\bar{\nu}_1}{E(\mathrm{ZPL})}\right]\left[\frac{\langle 0|n\rangle}{\langle 0|0\rangle}\right]^2 \qquad (9)$$

but the spectral congestion and overlapping of transitions hinders intensity measurements. An estimated 6 pm U−O bond length change upon excitation of **1** was obtained from this analysis. Comparison with the emission value gives the value 5 ± 1 pm for **1**.

Conclusions

The uranyl hypophosphites **1** and **2** both have structures built up by U−O−P−O−U links between uranyl groups with distorted pentagonal equatorial coordination. This leads to differently oriented polymeric chains in $UO_2(H_2PO_2)_2 \cdot H_2O$, and to a three-dimensional network structure in $UO_2(H_2PO_2)_2 \cdot H_3PO_2$, where H_3PO_2 plays the role of a unidentate terminal ligand. The vibrational spectra of both compounds are complex, with bands characteristic of the uranyl group and hypophosphite anion, and although not all of the predicted unit cell group splittings are resolved, the spectra are consistent with the crystallographic data. In particular, several bands enable the molecule H_3PO_2 to be distinguished from $H_2PO_2^-$ in **2**, although the OH group absorption is very weak. Both compounds exhibit weak luminescence because the excited uranyl ion can decay nonradiatively via excitation of 6−9 quanta of $\nu(OH_2)$ and ν(PH) modes. The luminescence spectra of **1** have been assigned and interpreted in detail, with comparisons of derived anharmonic constants and bond length changes upon excitation, to those of other uranyl systems. With this firm understanding of the structural and spectroscopic properties of **1** and **2**, the electronic absorption spectra up to the region near 29 000 cm^{-1} have been investigated. The two compounds are especially suitable in this respect because the foundations for the energy level scheme and electronic structure of the uranyl ion are built upon spectral measurements of systems in which UO_2^{2+} has high site symmetry: D_{2h} or D_{3h}.[3] More sparse data are available for D_{5h} symmetry systems[15] where the excited-state degeneracies and the transition selection rules are rather different. The distorted pentagonal bipyramidal coordination of uranium in the compounds **1** and **2** enables the model of Denning to be tested for the D_{5h} case. In particular the odd crystal field terms of the C_1 uranium site symmetry introduce electric dipole character into electronic transitions which are forbidden under D_{5h} selection rules, so that the transitions to parent $E_2''(D_{5h})$ excited states become prominent. Even though the electronic absorption spectra were recorded from mulls and polycrystalline samples, it turns out that all spectral features may be accommodated under Denning's model,[3] which assigns the excited states to those from the $\sigma_u\delta_u$ and $\sigma_u\phi_u$ configurations. For compounds **1** and **2**, the selection rules of transitions may differ considerably from those for $Cs_2UO_2Cl_4$, in which UO_2^{2+} occupies an approximately D_{2h} site. This is most notable for the transitions to the $\Gamma_g(D_{\infty h})$ excited states, XI,XII, which transform as A_g,B_{1g} (D_{2h}) and $E_1'(D_{5h})$, because the $A_{1g} \rightarrow E_1'(D_{5h})$ transition is electric dipole allowed and dominates the highest energy spectral region in **1** and **2**.

Acknowledgment. We thank Otto Ying-Tai Chan, Zhi-Wu Pei, Bo-Mu Wu, and Zhong-Yuan Zhou for technical assistance. Financial support from the Hong Kong Research Council Earmarked Grants CPHK 693/94P (P.A.T.), CUHK 303/96P (T.C.W.M.), and Strategic Research Grant 7000762 is gratefully acknowledged.

Supporting Information Available: Two X-ray crystallographic files, in CIF format. The 80 K emission spectra of **1** and **2**, electronic energy level diagrams, and a table summarizing the crystallographic data. This material is available free of charge via the Internet at http://pubs.acs.org.

IC990188R